Design and Analysis of Polarization Diversity Antenna for Mobile Terminals

Won-Woo Lee and Byung-Ho Rhee

This letter presents an antenna design method for an orthogonally-polarized dual antenna for use in mobile stations (MSs) and includes a verification method for improving the link-level throughput performance of an MS that uses a proposed multiple-input multiple-output antenna. The link-level throughput performance of an MS is strongly related to the correlation between antenna branches, which is determined by the cross polarization discrimination of the second branch antenna, both numerically and experimentally.

Keywords: Channel model, correlation, MIMO, polarization, throughput, XPD.

I. Introduction

Mobile stations (MSs) operating below 1 GHz face technical challenges when implementing mobile antennas with both a low correlation property and sufficient antenna gain [1]. If the isolation within the multi-antenna system is insufficient, system performance in terms of gain and correlation is reduced, due to the coupling effect between antennas. In general, an antenna coupling effect is always present in the antenna design for hand-held types of MSs, since the dual antennas share the same printed circuit board (PCB) [2].

This letter introduces a method for the design of an orthogonal polarization antenna for MSs using a planar inverted-F antenna. We use CST MICROWAVE STUDIO 2011 for the antenna design and obtain the current distribution for various antenna designs. In our design concept, the polarization state of the second branch antenna is adjusted by changing the distance between the signal and the ground feed launch point (GP).

Manuscript received June 12, 2013; revised Aug. 07, 2013; accepted Aug. 16, 2013.

Won-Woo Lee (phone: +82 10 9488 0822, wonwoo2.lee@gmail.com), Byung-Ho Rhee (corresponding author, bhrhee@hanyang.ac.kr) are with the Department of Electrics Computer Engineering, Hanyang University, Seoul, Rep. of Korea.

This letter also experimentally investigates the impact of second-antenna-branch cross polarization discrimination (XPD) on the antenna correlation characteristics by varying the polarization state of the second antenna branch. Comparisons of the downlink throughput performance of fabricated antennas are conducted through the physical downlink shared channel (PDSCH) throughput measurement of the 3GPP Long-Term Evolution (LTE) 2×2 multiple-input multiple-output (MIMO) system using the anechoic, chamber-based MIMO over-the-air (OTA) test, with methodology proposed in [3].

II. Antenna Design and Simulation

The antenna simulation is studied to derive the current flow distributions created by the dual antenna to see how the location of the GP in general folded inverted-F antennas affects the current flow distribution across the PCB. To study this, we design the antennas for a typical smartphone with an area of 60 mm × 130 mm. To adjust the polarization state of the sub-antenna, we design three types of sub-antennas with different GP locations, as shown in Fig. 1. The operating band of the antenna is band 5.

We utilize the equivalent dual antenna structure shown in

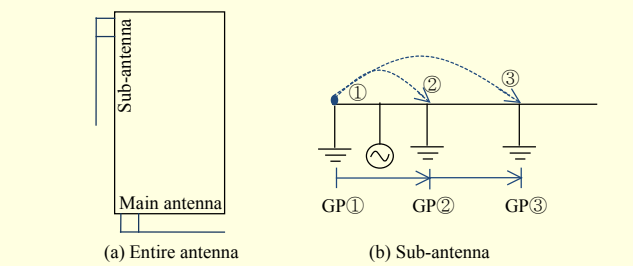

Fig. 1. Procedure for implementing structures.

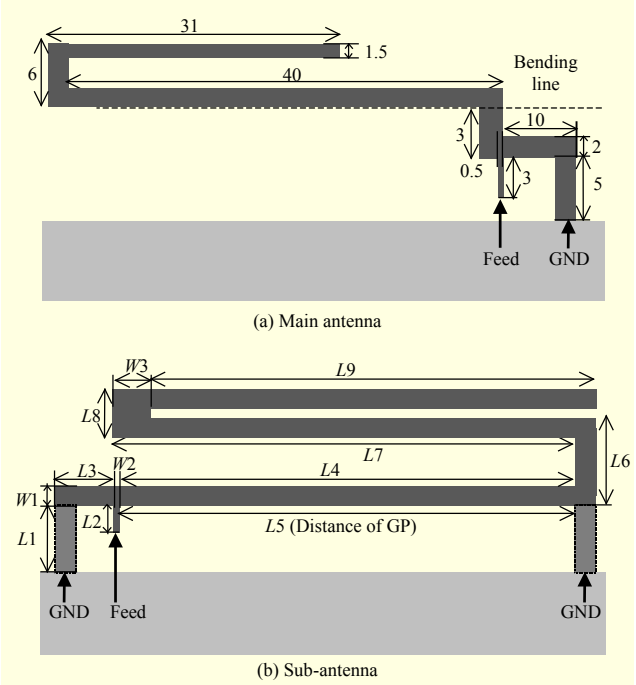

Fig. 2. Geometry of proposed antenna.

Table 1. Physical parameter values of proposed sub-antenna for GP.

Parameter	GP① (mm)	GP② (mm)	GP③ (mm)
L1	4.0	0	0
L2	3.0	3.0	3.0
L3	6.0	0	0
L4	43.5	49.5	49.5
L5	0	27.5	49.5
L6	6.0	6.0	6.0
L7	12.5	48.0	48.0
L8	0	5.5	5.5
L9	0	27.0	47.0
W1	2.0	0	0
W2	0.5	0.5	0.5
W3	0	3.0	3.0

Fig. 2. Detailed geometries of the main antenna structure are provided in Fig. 1(a). The physical parameters of the sub-antennas for the GP are presented in Table 1.

Figure 3 shows the simulation results of the dual antenna shown in Fig. 1(a). Simulations are carried out by changing the GP, as shown in Fig. 1(b), where the distance between the signal feed and the GP of the sub-antenna is varied. Figure 3(a) shows the induced current flows when the GP is located at ①. The current flow near the sub-antenna is in the vertical

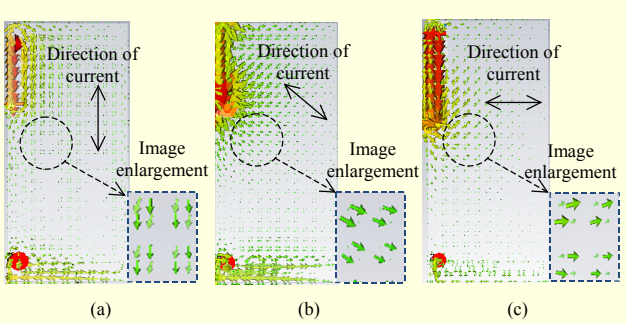

Fig. 3. Simulation result for switch of GP and current distributions for (a) GP①, (b) GP②, and (c) GP③.

direction. When the GP is at ②, we can see that the direction of current flow near the sub-antenna is tilted by approximately 45°, as shown in Fig. 3(b). Figure 3(c) shows the current distribution when the GP is at ③. The current flow direction is rotated until nearly horizontal.

III. Analysis through Fabricated Antenna

In this section, the three antenna types discussed in section II are realized to compare the measured results of XPD.

The XPD is obtained from the measured antenna patterns in 3-D space. It is found that the XPD and H-Pol gain are the key parameters for achieving a low envelope correlation coefficient (ECC).

The XPD is the ratio of the H-Pol gain to the V-Pol gain of the antenna patterns; thus, by using the XPD, the work herein verifies that an orthogonally-polarized dual antenna can be used in an MS to achieve desirable antenna performance. The XPD can be derived from (1) [4]. XPD is a pure antenna parameter and is used separately from the definition of cross polarization ratio (XPR).

$$\mathrm{XPD}=\frac{<G_{\Phi}>}{<G_{\theta}>}, \tag{1}$$

where G_{Φ} and G_{θ} represent the H-pol gain and the V-pol gain, respectively.

Figure 4 shows the XPD of the sub-antenna as a function of the elevation angle, θ, where all phi gain is an average value. When the GP is at ①, the XPD near the azimuth plane, or more precisely around $\theta = 90 \pm 15°$, is approximately –8 dB, meaning that the dominant polarization of the sub-antenna is V-pol. However, the XPD near $\theta = 90°$ is increasingly enhanced when the GP is at ② and ③. Particularly when the GP is at ③, the H-pol gain is larger than the V-pol gain, suggesting that the direction of current flows obtained from the simulations in section II explains the polarization states of the sub-antenna.

http://dx.doi.org/10.4218/etrij.14.0213.0280

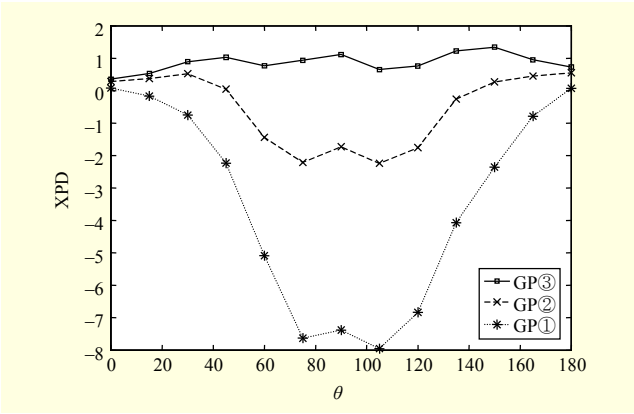

Fig. 4. Measured result of fabricated antenna for average XPD characteristics as function of theta.

IV. Performance Verification Using the MIMO OTA System

This chapter applies the geometrical channel model to numerically estimate the performance of the MIMO antennas and to verify the correlation and link-level throughput performance of the MIMO OTA system. The 3GPP Spatial Channel Model Extension (SCME) Urban Macro (UMa) [5] is used for the geometrical channel model, as the angular positions of the clusters are widely spread over the azimuth plane. Note that SCME UMa is one of the channel models being used in the 3GPP RAN4 MIMO OTA round-robin test activities [3].

The MIMO OTA system diagram is shown in Fig. 5. The system creates a 2-D Laplacian power azimuth spectrum in the azimuth plane using channel models. To do this, the V-pol and H-pol components need to be transmitted independently so that the XPR of the radio channel can be modeled. There are dual polarized 8-OTA antennas, which are arranged uniformly at a 45° angular distance in the azimuth plane. 2×2 LTE MIMO signals are generated at the LTE Base Station Emulator (BSE), and are fed to the fading emulator. In this way, a spatiotemporal fading channel environment is created at the center of the chamber.

Measurement of antenna correlation using the MIMO OTA system is possible if we measure the power correlation from the received signal powers through the antenna under test (AUT). To do this, we use a vector signal analyzer (VSA) to sample the signals from the AUT, as shown in Fig. 5. The power correlation coefficient between time samples of the received power from the two antenna branches is given by

$$\rho_{\text{pwr}} = \left| \frac{E\{P_1 \times P_2 + P_2 \times P_1\}^2}{E\{P_1 \times P_1\}E\{P_2 \times P_2\}} \right|, \quad (2)$$

$$P_1 = FFT(S_1), \quad P_2 = FFT(S_2). \quad (3)$$

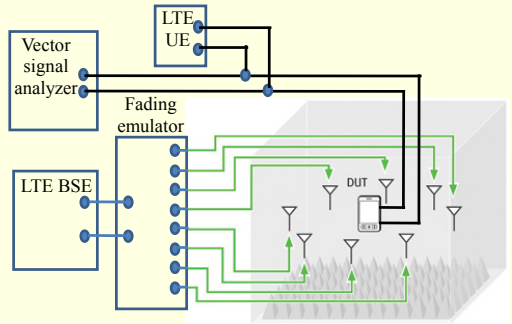

Fig. 5. MIMO OTA system diagram for correlation and throughput measurement with application of channel model.

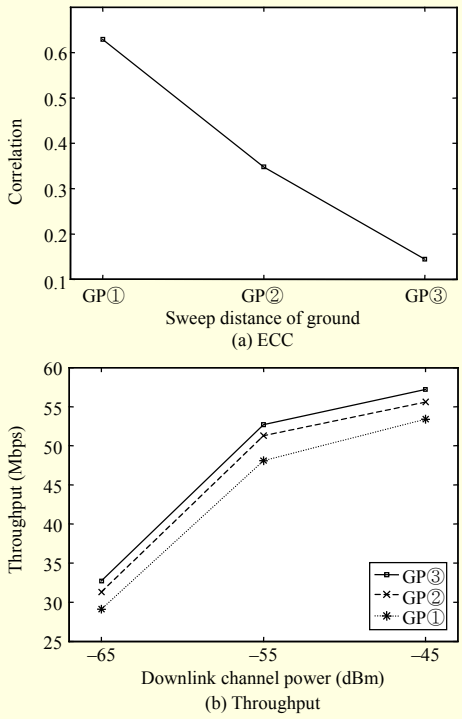

Fig. 6. Measurement results for channel model of SCME UMa measured in MIMO OTA system.

S_1 and S_2 denote the received signals, P_1 and P_2 denote the received power, and ρ_{pwr} denotes the power correlation measured by the VSA. It should be noted that the power correlation coefficients are an approximation of the squared amplitudes of the complex signal correlation [6].

Figure 6 shows the measured power correlation and throughput results for the three types of AUTs using the MIMO OTA system. The measurement results are averaged over four different device orientation angles in the azimuth plane. The broad side of the device is set to 0°, 90°, 180°, and 270° for every test run and averaged. The measured power correlation from the MIMO OTA system is shown in Fig. 6(a). The ECC is the value measured by the VSA of the MIMO OTA system

based on (2) and (3). It should be noted that the antenna correlation decreases as the GP moves from GP① to GP③. When the GP is at ③, the ECC is further reduced as the dominant polarization of the sub-antenna.

Figure 6(b) shows the measurement results of the LTE physical layer throughput performance as a function of the average downlink channel power in the MIMO OTA system. The measurements are conducted based on the parameters summarized in Table 2. The LTE PDSCH throughput is measured over a power range of –45 dBm to –65 dBm/9 MHz. In general, a high modulation and coding scheme (MCS) is associated with low correlation. Even with a high MCS, a high terminal correlation value leads to lower max throughput performance. We utilize a method that locates a max throughput, while changing the MCS. The maximum MCS is determined while maintaining the block error rate counts from the cyclic redundancy check error of the media access control packet data unit below 10%. The performance is primarily dependent upon the correlation properties of antennas, as long as the power loss at the antenna does not affect the SNR. Through the throughput performance comparison of the AUTs, we show that the AUT with the lowest correlation shows higher throughput than the other AUTs over the entire downlink signal power range. The underlying mechanism is the increase in mutual information of the radio link as the correlation between the Rx main antenna and sub-antenna is reduced [7]. It should be noted that the throughput drop observed at GP② and GP③ is larger than the throughput decrease experienced at GP① and GP②, meaning that the throughput performance degradation is more significant in high correlation ranges than in low correlation ranges.

Table 2. Parameter for MIMO OTA performance measurement.

Parameters	Description
LTE frame structure	FDD with normal CP
System bandwidth	10 MHz
RF allocation	DL: 50, UL: 12
Frequency	DL: 881.5 MHz, UL: 836.5 MHz
Total BS transmit power	– 45 dBm - – 65 dBm/9 MHz
PDSCH transmission mode	TM3 (Open loop spatial multiplexing)
PDSCH MCS	Variable (MCS index = 0 - 28)
KTB·NF	– 97.5 dBm/9 MHz
Channel model	SCME UMa (non-line-of-sight)
BSE	E6621A (Agilent PXT wireless communications test set)
LTE receiver	LG-SU640 (Qualcomm modem chipset: MDM9200)

V. Conclusion

In this letter, we presented an antenna design concept in which the H-pol gain of the sub-antenna can be enhanced by separating the signal launch point and the GP of the sub-antenna element, when its location is on the top or side of the PCB. We also show that the enhanced XPD of the sub-antenna significantly reduces the ECC of the dual antenna of the MS.

In this letter, we confirmed that the polarization of the dual antenna should be orthogonal or, equivalently, the XPD of the sub-antenna should be enhanced as much as possible to improve the link-level throughput performance of the MS. It is clear that the link-level throughput performance of the AUT is enhanced as the XPD of the sub-antenna is increased due to the reduced correlation between the dual-antenna, which enhances the mutual information of the radio channels.

References

[1] P. Vainikainen et al., "Recent Development of MIMO Antennas and Their Evaluation for Small Mobile Terminals," *17th Int. Conf. Microw., Radar, Wireless Commun.*, Wroclaw, Poland, May 19-21, 2008, pp. 1-10.

[2] T. Ohishi et al., "A Method to Improve the Correlation Coefficient and the Mutual Coupling for Diversity Antenna," *IEEE Antennas Propag. Soc. Int. Symp.*, vol. 1A, July 3-8, 2005, pp. 507-510.

[3] 3GPP TR 37.976, "Measurement of Radiated Performance for MIMO and Multi-antenna Reception for HSPA and LTE Terminals," (Release 11), version 1.5.0, May 2011.

[4] Y. Okano and K. Cho, "Dependency of MIMO Channel Capacity on XPR Around Mobile Terminals for Multi-band Multi-Antenna," *Proc. 2nd European Conf. Antennas Propag.*, Edinburgh, UK, Nov. 11-16, 2007, pp. 1-6.

[5] D.S. Baum, J. Hansen, and J. Salo, "An Interim Channel Model for Beyond-3G Systems: Extending the 3GPP Spatial Channel Model (SCM)," *Proc. 61st IEEE Veh. Technol. Conf.*, vol. 5, Stockholm, Sweden, May 30-June 1, 2005, pp. 3132-3136.

[6] Y. Karasawa and H. Iwai, "Modeling of Signal Envelope Correlation of Line-of-Sight Fading with Applications to Frequency Correlation Analysis," *IEEE Trans. Commun.*, vol. 42, no. 6, June 1994, pp. 2201-2203.

[7] Y.S. Cho, P. Kyösti, and I.K. Kim, "Characterization of MIMO OTA Link Level Performance of Dipole Antenna Array," *Proc. 7th European Conf. Antennas Propag.*, Gothenburg, Sweden, Apr. 8-12, 2013, pp. 2549-2553.